Direct Multivariable Control for Modular Multilevel Converters

Daniel Dinkel, *Member, IEEE*, Claus Hillermeier, and Rainer Marquardt, *Member, IEEE*

***Abstract*—Modular multilevel converters (MMCs) have enabled new and demanding applications for power electronics in the high voltage/high power range. In these applications, very fast and tight control of all variables of the MMC is of prime importance. This article presents a new multivariable control (MVC) concept, which enables independent and extremely fast control of all essential variables. For each variable, a tolerance band can be specified, which is strictly met even under unexpected severe transients and disturbances. The minimized dead times achieved by the control are more than one order of magnitude smaller than the state of the art. The MVC has been implemented based on FPGA-hardware and digital signal processing of the measured values. Experimental results of the control performance and the robustness against parameter variation are presented, using a down scaled MMC with 96 submodules. These results include the analysis of steady-state operation, dynamic performance, and fault scenarios.**

***Index Terms*—Control theory, dc grids, fault handling, modular multilevel converters (MMC), multiterminal HVdc, multivariable control, VSC.**

I. Introduction

MODULAR multilevel converters (MMCs) are the key components in many existing and emerging high power system applications [1], [2], such as wind or photovoltaic energy conversion systems [3], high voltage direct current (dc) transmission systems [4], electric ships [5] and multiterminal dc grids [6], [7]. In all these applications—in particular, in possible multiterminal dc grids—MMCs will increasingly have the task to control and to electronically protect the associated alternating current (ac) and dc grids and themselves, even during fast transients and unexpected severe fault conditions. These requirements include the necessary capability of short-circuit current limitation and will become important because tripping of mechanical switches or blocking of the converters after faults is unacceptable or undesirable. A control concept meeting these prospective demands has to control the alternating and direct currents *directly*, and this current control has to operate with minimized control dead times of less than 10 μs (typically 5μs) and a control bandwidth larger than 100 kHz. These requirements are more than one order of magnitude tighter than the state-of-the-art MMC control.

In addition, the stored energies of the MMCs have to be stabilized and controlled independently of the external operating conditions. Balancing of the internal arm energies is the task of a high-level controller and is done by shaping reference trajectories for three MMC-internal variables, namely the circulating current (cc) space vector (two variables) and the common-mode (cm) voltage. Thus, in order to enable a fast and tight control of the internal arm energies, the cc and the cm-voltage should additionally be controlled with high bandwidth and minimized delay time. In consequence, essential reductions of capacitor size and of chokes can be achieved. Such an approach can also provide overcurrent protection of the semiconductors in the MMC.

A new control method meeting all these tough demands is presented in this article. It is called *direct multivariable control* (MVC). In order to achieve the required dead times, MVC has to be embedded into a control hierarchy with a strict assignment of tasks. In such a design, the task of controlling dynamical processes, which are slow (compared to the current dynamics), is assigned to an upper level controller (ULC). Table I gives the position of the MVC within such a layered structure of MMC control.The MVC receives its target values from the ULC. Control layer 3 provides target values for the alternating and direct currents. Layer 2, which controls and balances the internal arm energies of the MMC, specifies the target values for the cc and the cm-voltage.

In summary, MVC controls the following six variables simultaneously with high bandwidth and independently from each other: 1) dc; 2) ac (two independent variables forming a space vector); 3) cc (two independent variables forming a space vector); and 4) cm voltage. Thus, all degrees of freedom in MMCs

TABLE I
Control Layers of the MMC and Associated Tasks

Layer	Function	Name
3	Control of ac- and dc-grid values and of the total converter energy	Upper level control (ULC)
2	Control of the arms energy distribution	
1	Multivariable control (MVC)	Lower level control (LLC)
0	Submodule capacitor sorting/balancing	

Manuscript received August 6, 2021; revised December 16, 2021; accepted January 21, 2022. Date of publication February 7, 2022; date of current version March 24, 2022. This work was supported by the FORscience Research Fund of the University of the Bundeswehr Munich. Recommended for publication by Associate Editor F. Dijkhuizen. *(Corresponding author: Daniel Dinkel.)*

Daniel Dinkel and Claus Hillermeier are with the Department of Electrical Engineering and Information Technology, Chair of Automation and Control Engineering, University of the Bundeswehr Munich, 85579 Neubiberg, Germany (e-mail: daniel.dinkel@unibw.de; claus.hillermeier@unibw.de).

Rainer Marquardt is with the Department of Electrical Engineering and Information Technology, Emeritus of Excellence, University of the Bundeswehr Munich, 85579 Neubiberg, Germany (e-mail: rainer.marquardt@unibw.de).

Color versions of one or more figures in this article are available at https://doi.org/10.1109/TPEL.2022.3148578.

Digital Object Identifier 10.1109/TPEL.2022.3148578

are controlled by the MVC. The output of the MVC is a switching decision. It is sent to layer 0, which finally selects the submodule (SM) to be switched—based on a sorting algorithm.

A. Brief Summary of Existing MMC Control Approaches

Existing methods for the control of an MMC can be categorized roughly into two groups, called group A and group B in the following [8], [9]. The methods of group A consist of a high-level controller, which is combined with a modulation and SM selection scheme. Group B methods perform the whole MMC control within one model predictive control (MPC) step.

In group A methods, the high-level control is essentially responsible for the tasks of control layers 3 and 2, as given in Table I. The approaches used for this high-level control task range from multiple PI-controllers over MIMO control techniques and MPC to advanced nonlinear control methods [4], [10]–[14]. As a common characteristic of group A control methods, all target trajectories for *currents*, which are generated in some stage of the high-level control have to be translated (by means of current control loops) into target values of *voltages*. A subordinate modulation and SM selection scheme then tries to adjust these voltages by creating appropriate gating signals for the semiconductor switches. Thus, superposed current control loops are a necessary prerequisite for applying modulation schemes. This fact seriously restricts the bandwidth and performance of group A methods with respect to current control.

Three widely used types of modulation schemes are nearest-level-modulation methods with additional voltage PWM [15]–[19], space vector modulation methods [20]–[22], and carrier based methods [23]–[26]. All these schemes are introducing the extra dead times of the modulators, and the performance and bandwidth of current control are additionally impaired by the errors of voltage control. Although modulation methods try to minimize the current errors by employing smart switching schemes, they are, by design, not able to keep all current errors within predefined limits in all dynamic situations.

B. Differences Between MPC-Based MMC Control and MVC

An alternative approach to MMC control is the MPC concept [12], [27], [28]. In contrast to group A methods, MPC eliminates the necessity of cascaded current and voltage control, and thus, improves the dynamic performance and controllability as compared to group A control methods. MPC achieves multiple objectives for MMC control by including these objectives in a single cost function. In the purest form of this concept, the cost function is evaluated for all possible switching states, and the optimal switching state is selected and applied to the MMC. Algorithms of this kind are called optimal switching state-based MPC (OSS-MPC) in the literature, and have been denoted group B methods previously. Depending on the used mathematical model of MMC, the MPC literature distinguishes between per-phase and three-phase MPC methods. Since only three-phase methods allow for the control of cc, solely algorithms of this type are regarded further. For three-phase OSS-MPC, the number of switching states, for which the cost function has to be evaluated, increases exponentially with the number of SMs per arm. This computational complexity makes it impossible to employ OSS-MPC for higher numbers of SMs per arm, especially for HVdc. In order to reduce the computational burden, a lot of other MPC-based algorithms have been devised. One strategy is to optimize a cost function in order to identify the best switching vector, which only specifies the number of inserted SMs in each arm. This can be considered as a simplified method to determine a target value of the arm voltage.

By eliminating the cascaded current and voltage control loops, MPC improves the dynamic performance and achieves fast responses during transients [29]. Yet, the optimization that has to be done within each time step has a computational complexity, which makes it nearly impossible to work with sampling periods shorter than 50–100 μs. Compared to this, the presented MVC is characterized by control dead times, which are smaller by more than one order of magnitude. In view of the abovementioned future requirements of MMC, this is a substantial progress.

Another striking difference between the MPC and the MVC concepts is due to the very principle of MPC to include multiple control objectives in a single cost function. This cost function is mainly a weighted sum of the quadratic errors of the variables to be controlled and comprises other objectives, such as the switching frequency. Thus, the calculated optimum just minimizes the mean squared error of all the variables to be controlled, but cannot guarantee that each single variable is always kept within a tight tolerance band around its reference trajectory. In contrast, this is exactly what the presented MVC ensures for the ac space vector, the cc space vector, the dc, and the cm voltage.

A variant of MPC called model predictive direct current control [30] manages to maintain the ac within tight bounds by introducing additional constraints. The corresponding optimization problem includes the ac errors not in the form of cost function summands, but in the form of constraints, which require that all feasible solutions have ac errors within certain bounds (tolerance bands). Although this MPC variant achieves a direct ac current control, the other control variables are still included in the form of contributions to the cost function—after all, the central role of a cost function is what makes up any MPC algorithm. Thus, even MPC approaches of this kind are not able to ensure that all six essential variables of MMC are simultaneously kept within tight tolerance bands around their target trajectories. For the variant presented in [30], the optimization problem to be solved in each time step requires a sampling period of 125 μs.

Some MPC approaches rely on a subordinate modulation and/or SM selection scheme [28], [31], [32]. In the framework of the classification made previously, these algorithms belong to the control methods of group A, except for the fact that no additional current control loops are used. For the strongly increased dynamic challenges tackled by MVC, these MPC algorithms are not appropriate since all what has been stated previously about modulation schemes (dead time of modulator) and about MPC (cost function consisting of weighted errors, sampling period due to computational complexity) applies also to them.

C. Important Features of the Presented MVC

In the following, a short summary will be given of the most important features of MVC and its differences to state-of-the-art control approaches.

1) Based on arm current measurements, all six degrees of freedom in an MMC, namely the ac space vector, the cc space vector, the dc, and the cm voltage, are directly controlled by MVC. Even in any dynamic situation, each of these variables is individually kept within a small, predefined tolerance band around its reference value.
2) This is achieved by adjusting the driving voltages, whenever necessary, by utilizing small incremental voltage corrections. MVC does not use a fixed sampling period. On the contrary, the switching frequency is perfectly adjusted to the actual dynamical situation. During transient—or, even, faulty—conditions, a large number of switching actions can be applied, whereas in steady-state operation a low switching frequency is assured.
3) A set of 28 switching options is preselected, and their effect on all six variables can be analyzed and optimized offline and stored in a lookup table. This makes the switching decision extremely fast. Minimal dead time (typically 5 μs) and very high control bandwidth (> 100 kHz) of the current control are achieved in this way.
   (Since the MVC concept does not apply a fixed sampling period, the term control bandwidth is used here just to relate the time scale of MVC to the frequencies of the dynamics to be controlled.)
4) MVC with defined tolerance bands does *not* mean that the control has to operate in the manner of a hysteresis control. When one of the six variables to be controlled touches its tolerance band, an appropriate switching action is initiated. The MVC makes its switching decision based on the way all six variables move *inside* their tolerance bands due to the switching.
5) MVC generates very smooth current signals because it is able to minimize not only the current errors but also the di/dt errors simultaneously. The decision of using current measurements as primary inputs is discussed in the Appendix.
6) The computational complexity of MVC does not increase with increasing number of SMs.
7) The control method relies on local measurements within the MMC and is robust against uncertainties and changes of external system and grid parameters.
8) Whereas modulation schemes are strongly impaired by voltage ripples of the capacitors, this is not the case for MVC. Since a reduction of SM capacitances translates the unavoidable oscillations of the arm energies into significant oscillations of the capacitor voltages, the insensitivity of MVC to such capacitor voltage ripples gives the option of further minimizing SM capacitances.
9) The tight and fast control of all currents within the MMC arms enables an essential reduction of the arm inductances.

Preliminary versions of the MVC concept have been published in [33]–[35].

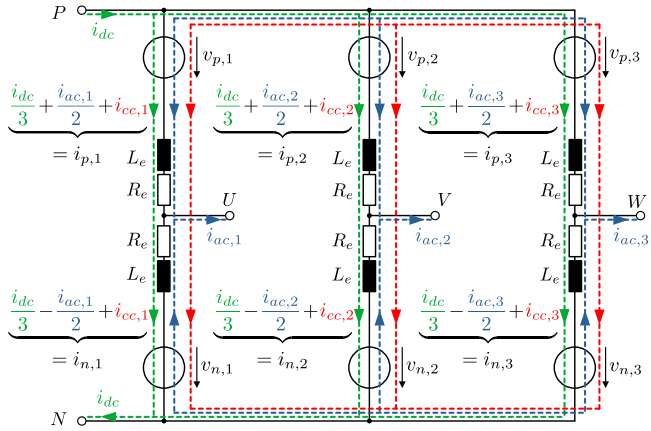

Fig. 1. Structure of MMC with highlighted dc i_{dc}, ac $i_{\mathrm{ac},1/2/3}$ and cc $i_{\mathrm{cc},1/2/3}$.

II. Description of the MMC

A. Structure and Variables

Fig. 1 shows the known basic structure of an MMC. It consists of three phase legs labeled by j, $j \in \{1, 2, 3\}$, each composed of an upper (positive) and a lower (negative) arm indexed with p and n, respectively. Any arm contains tens to hundreds SMs, including capacitors as storage devices. Although the MVC concept is not principally restricted to a certain SM topology, the present analysis assumes SM of bipolar type, such as full bridge or advanced topologies, as discussed in Section IV. The arm voltages of the positive and negative arms are denoted as $v_{p,j}$ and $v_{n,j}$, respectively. Currents i_{dc} and $i_{\mathrm{ac},1/2/3}$ flow through the dc and ac terminals, respectively. As the three alternating currents add up to zero, they can be represented by a two-component space vector. Each arm current $i_{p/n,j}$ contains—apart from the dc and ac parts—a third component, which is internal to the MMC, the cc $i_{\mathrm{cc},j}$. The cc $i_{\mathrm{cc},1/2/3}$ add up to zero and, therefore, are represented by a two-component space vector, too. The arm impedance is summarized by resistance R_e and inductance L_e. Here, the value of the arm inductance L_e is an important design parameter. The arm resistances R_e are small and would, when considered in the mesh equations, result in small contributions to the counter voltages (see below). Since these counter voltage contributions largely cancel out in the error terms, on which the MVC is based, the resistances R_e will be neglected in the subsequent model of the dynamics.

The external grids are in general quite complex, as is illustrated by the exemplary grid model shown in the upper part of Fig. 2. It is neither desirable nor feasible to model all parts of such an extended grid and to identify all of its parameters, which are prone to changes. For the stable operation of the presented MVC, a linear model is necessary and sufficient, which is just valid for the short time span between two corrective switching decisions of the MVC. This requirement can be met by an extremely simplified grid model, consisting of an equivalent inductance and an equivalent counter voltage, as shown in Fig. 2. Both parameters of this reduced model are virtual values not related to any real component. The equivalent inductance of this

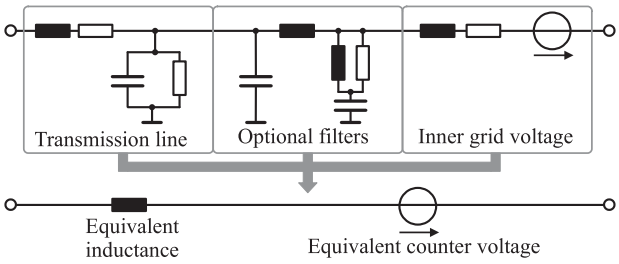

Fig. 2. Complex external grids [36], [37] can be modeled as an equivalent inductance and an equivalent counter voltage.

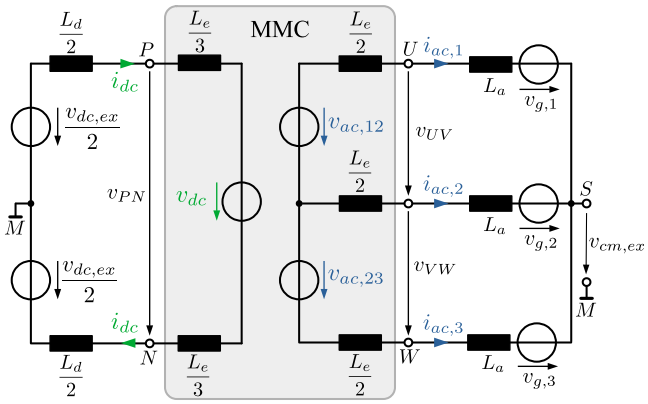

Fig. 3. Current loops (dc and ac) with highlighted internal (gray) and external part.

model is not identical to the inductance at the fundamental line frequency, which could be derived from the known power factor, for example. One option to determine the equivalent inductance is an impedance measurement with a test frequency similar to the average switching frequency of the MVC. In the presented setup, this is a frequency in the 30-kHz range. The MVC scheme also allows for online adaptation of the value of the equivalent inductance during normal operation. Each time a known SM capacitor voltage is switched, a comparison between estimated and measured values of current derivatives di/dt can be used to adapt the values of the equivalent inductances of the external grids. The operation of the MVC is not sensitive to moderately inaccurate values of the equivalent inductances. Errors in a range of $\pm 40\%$ do not have any significant impact, as is proven by experimental results shown in Section IV-D.

The second parameter, the equivalent counter voltage, incorporates the contribution of voltage sources, ohmic voltage drops, and voltages of capacitors (i.e., filter capacitors) in the short time span between two switching decisions of the MVC. During this time span, all these parts of the voltage do not vary considerably. Therefore, the best estimation of the equivalent counter voltage is the arithmetic mean value of this voltage during this short time span.

B. Dynamics

Using the above-mentioned simplified grid model, each of the six arms shown in Fig. 1 can be completed by external system parts of Fig. 3 to form a loop. The corresponding mesh equations give the dynamics of the six arm currents, $j \in \{1,2,3\}$

$$v_{p,j} = \frac{v_{\mathrm{dc},ex}}{2} - \frac{L_d}{2}\frac{\mathrm{d}i_{\mathrm{dc}}}{\mathrm{d}t} - L_e\frac{\mathrm{d}}{\mathrm{d}t}\left(\frac{i_{\mathrm{dc}}}{3} + \frac{i_{\mathrm{ac},j}}{2} + i_{\mathrm{cc},j}\right) - v_{g,j} - v_{\mathrm{cm},ex} - L_a\frac{\mathrm{d}i_{\mathrm{ac},j}}{\mathrm{d}t} \quad (1)$$

$$v_{n,j} = \frac{v_{\mathrm{dc},ex}}{2} - \frac{L_d}{2}\frac{\mathrm{d}i_{\mathrm{dc}}}{\mathrm{d}t} - L_e\frac{\mathrm{d}}{\mathrm{d}t}\left(\frac{i_{\mathrm{dc}}}{3} - \frac{i_{\mathrm{ac},j}}{2} + i_{\mathrm{cc},j}\right) + v_{g,j} + v_{\mathrm{cm},ex} + L_a\frac{\mathrm{d}i_{\mathrm{ac},j}}{\mathrm{d}t}. \quad (2)$$

Forming the sum and the difference of (1), (2) decouples the dynamics of the dc and the cc from the dynamics of the ac

$$v_{p,j} + v_{n,j} = v_{\mathrm{dc},ex} - \left(L_d + \frac{2L_e}{3}\right)\frac{\mathrm{d}i_{\mathrm{dc}}}{\mathrm{d}t} - 2L_e\frac{\mathrm{d}i_{\mathrm{cc},j}}{\mathrm{d}t} \quad (3)$$

$$\frac{v_{p,j} - v_{n,j}}{2} = -v_{g,j} - v_{\mathrm{cm},ex} - \left(L_a + \frac{L_e}{2}\right)\frac{\mathrm{d}i_{\mathrm{ac},j}}{\mathrm{d}t}. \quad (4)$$

Due to $i_{\mathrm{cc},1} + i_{\mathrm{cc},2} + i_{\mathrm{cc},3} = 0$, summing (3) over all three phases results in the pure dc dynamics

$$\sum_{y=1}^{3}\frac{v_{p,y} + v_{n,y}}{3} = v_{\mathrm{dc},ex} - \underbrace{\left(L_d + \frac{2L_e}{3}\right)}_{L_{\mathrm{dc}}}\frac{\mathrm{d}i_{\mathrm{dc}}}{\mathrm{d}t} = v_{\mathrm{dc}}. \quad (5)$$

Applying (5) to (3) gives the dynamics of the cc

$$\sum_{y=1}^{3}\frac{v_{p,y} + v_{n,y}}{2} - \frac{3}{2}\left(v_{p,j} + v_{n,j}\right) = \underbrace{3L_e}_{L_{\mathrm{cc}}}\frac{\mathrm{d}i_{\mathrm{cc},j}}{\mathrm{d}t} = v_{\mathrm{cc},j}. \quad (6)$$

Forming the difference of (4) between two converter phases j and k, gives

$$v_{\mathrm{ac},jk} - (v_{g,j} - v_{g,k}) = \underbrace{\left(L_a + \frac{L_e}{2}\right)}_{L_{\mathrm{ac}}}\frac{\mathrm{d}i_{\mathrm{ac},jk}}{\mathrm{d}t}$$

$$v_{\mathrm{ac},jk} = \frac{-v_{p,j} + v_{n,j} + v_{p,k} - v_{n,k}}{2}$$

$$i_{\mathrm{ac},jk} = i_{\mathrm{ac},j} - i_{\mathrm{ac},k} = i_{p,j} - i_{n,j} - i_{p,k} + i_{n,k}. \quad (7)$$

Hence, a pure ac dynamics equation, without involving the external cm voltage $v_{\mathrm{cm},ex}$, is achieved. Equations (5)–(7) describe the dynamics of the five currents to be controlled by the MVC. The shaded box of Fig. 3 illustrates those parts of the equivalent circuits that are internal to the MMC. As can be seen, the arm inductances L_e contribute to the effective inductances L_{dc} and L_{ac} in (5) and (7), respectively. However, the external inductances L_d and L_a may fluctuate in certain network scenarios, the value of L_e is fixed during the MMC design. Thus, the L_e-correlated contribution to L_{dc} and L_{ac} maintains the assumed inductive behavior of the external current dynamics even in the case of a significant decrease of L_d or L_a. Fig. 3 demonstrates the distinction between the voltage v_{dc} driving (together with $v_{\mathrm{dc},ex}$) the dc, and the voltage v_{PN} at the dc-terminal of the MMC. The analogous distinction between, e.g., $v_{\mathrm{ac},12}$ and the terminal voltage v_{UV} can be seen at the ac-side of the MMC.

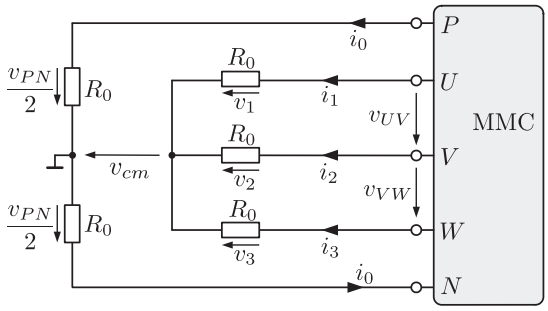

Fig. 4. Circuit to define v_{cm} ($R_0 \to \infty$).

The MVC concept does not rely on a special structure of the connected ac grid, and no detailed knowledge about this external grid structure has to be assumed. Thus, the external cm voltage $v_{\mathrm{cm},ex}$ (as shown in Fig. 3, in an exemplary way) is not an appropriate variable to be controlled. Instead, the circuit shown in Fig. 4 allows to define the cm voltage v_{cm} of the ac terminals, which is important for balancing the arm energies and will, therefore, be controlled by the MVC. Replacing the external ac parts in (1) and (2) by the corresponding parts of this measurement circuit and summing up the differences for all three phases gives

$$\sum_{y=1}^{3} \frac{v_{n,y} - v_{p,y}}{6} = v_{\mathrm{cm}}. \tag{8}$$

III. Direct MVC Concept

The target values for the six variables to be controlled, i_{dc}, $i_{\mathrm{ac},1}$, $i_{\mathrm{ac},2}$, $i_{\mathrm{cc},1}$, $i_{\mathrm{cc},2}$, and v_{cm}, are sent to the MVC by the upper level controller (ULC). (Note that $i_{\mathrm{ac},3} = -i_{\mathrm{ac},1} - i_{\mathrm{ac},2}$ and $i_{\mathrm{cc},3} = -i_{\mathrm{cc},1} - i_{\mathrm{cc},2}$ are dependent variables.) The task of the MVC is to keep all six variables in specified tolerance bands around their target values at all times and under all circumstances, i.e., even under transient and fault conditions. In order to meet this requirement, the MVC appropriately adjusts the driving voltages for the current dynamics by generating commands for the switching of SMs.

A. Signal Flow Within the MVC

Fig. 5 illustrates the concept of the MVC by means of signal flows. The MVC receives as input signals the target (or "reference") values (labeled with *), and the measured values for the five currents to be controlled. It also obtains the estimated time derivatives of these current signals. All these values are based on the measurements of the arm current transducers. The estimation of the derivatives is technically challenging and is explained in the Appendix. Further inputs to the MVC are the target value of the cm voltage v^*_{cm} and the values of the six arm voltages, which allow for computing the actual value of v_{cm}.

As a first step, the differences between target and measured values, i.e., the control errors, are formed and denoted by Δ

$$\Delta i_{\mathrm{ac},jk} = i^*_{\mathrm{ac},jk} - i_{\mathrm{ac},jk}$$
$$\Delta i_{\mathrm{cc},j} = i^*_{\mathrm{cc},j} - i_{\mathrm{cc},j}$$
$$\Delta i_{\mathrm{dc}} = i^*_{\mathrm{dc}} - i_{\mathrm{dc}}$$
$$\Delta v_{\mathrm{cm}} = v^*_{\mathrm{cm}} - v_{\mathrm{cm}}. \tag{9}$$

The information about target and measured values of the *time derivatives* of ac, cc, and dc can be used to reconstruct the errors of the driving voltages. For that purpose, (5)–(7) are written once for the target time derivative and once for the measured (estimated) time derivative. Forming the difference of these equations gives error expressions for the driving voltages, which no longer contain the counter voltages considered to be only known with uncertainty.

$$\Delta v_{\mathrm{ac},jk} = v^*_{\mathrm{ac},jk} - v_{\mathrm{ac},jk} = L_{\mathrm{ac}} \left(\frac{\mathrm{d}i^*_{\mathrm{ac},jk}}{\mathrm{d}t} - \frac{\mathrm{d}i_{\mathrm{ac},jk}}{\mathrm{d}t} \right)$$
$$\Delta v_{\mathrm{cc},j} = v^*_{\mathrm{cc},j} - v_{\mathrm{cc},j} = L_{\mathrm{cc}} \left(\frac{\mathrm{d}i^*_{\mathrm{cc},j}}{\mathrm{d}t} - \frac{\mathrm{d}i_{\mathrm{cc},j}}{\mathrm{d}t} \right)$$
$$\Delta v_{\mathrm{dc}} = v^*_{\mathrm{dc}} - v_{\mathrm{dc}} = -L_{\mathrm{dc}} \left(\frac{\mathrm{d}i^*_{\mathrm{dc}}}{\mathrm{d}t} - \frac{\mathrm{d}i_{\mathrm{dc}}}{\mathrm{d}t} \right). \tag{10}$$

Thus, the information about the errors of the driving voltages is based on derivatives of measured current signals. The conversion of derivative errors into voltage errors is done by means of effective inductances for the external loops, which are not precisely known. Therefore, the robustness of the MVC against coarsely mistuned values of these parameters has been investigated in Section IV-D.

The alternating currents and driving voltages as well as the circulating currents and driving voltages form three-phase systems without zero component, a property that is passed on to the respective errors. Therefore, the next processing step consists of Clark transforming both the ac and cc errors and the ac and cc voltage errors, resulting in four error space vectors.

An important issue of the MVC scheme is the definition of an interval of tolerated errors, called *tolerance band*, for each variable to be controlled. As shown in Fig. 6, the tolerance bands are modeled by circles for the ac and cc space vectors and as intervals for the scalar variables i_{dc} and v_{cm}. The errors of the voltages, which drive the five currents (ac, cc, and dc), indicate the future trends of the current errors. To enable a fast and tight current control and to achieve smooth waveforms of the current signals, tolerance bands must also be defined for the errors of the driving voltages (see Fig. 6). All errors are normalized with respect to their predefined tolerance bands. For the ac, cc, and dc variables, a total error (denoted by e) is determined as a weighted sum of the current and the voltage error. The control decisions to be taken can be based on two error space vectors $\underline{e}_{\mathrm{ac}}$ and $\underline{e}_{\mathrm{cc}}$ and two scalar-valued errors e_{dc} and e_{cm}.

First, the errors are compared to their tolerance bands. Any time, when one of the tolerance bands is touched, the MVC decides to generate a correcting control voltage vector. The decision for the best control voltage and the corresponding switching command is guided by the following considerations.

1) Two space vector errors and two scalar errors have to be taken into account simultaneously (six variables).
2) The number of switching commands (for the semiconductors) shall be minimized.

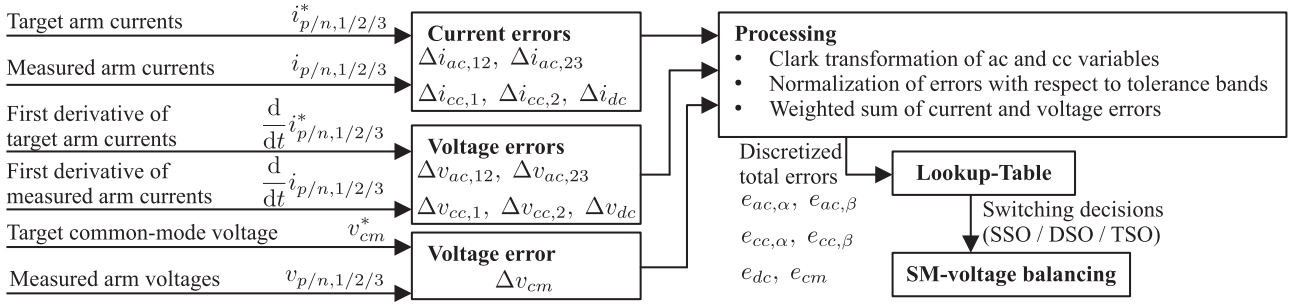

Fig. 5. Signal flow diagram of the MVC.

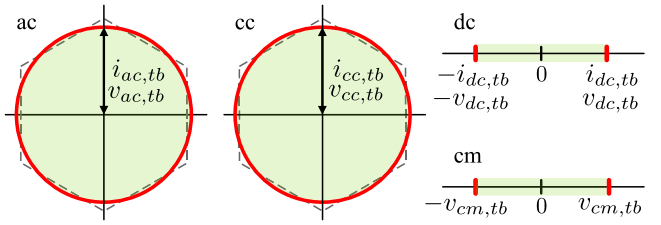

Fig. 6. Circle-shaped tolerance bands for ac and cc components (currents and voltages). Scalar tolerance bands for the dc component (current and voltage) and cm voltage.

3) The magnitude of the control voltages should be minimized in normal operation, since a too small magnitude can always be corrected by quickly repeating the same control vector.

In the next section, it will be explained how the decision algorithm is implemented according to these guidelines.

The switching decision of the MVC can be expressed as the label of the arm(s), where a SM capacitor voltage has to be switched, including the polarity of the switching. This information is sent by the MVC to the lowest level control (see layer 0 of Table I), which is responsible for a final SM selection.

B. Table of Predefined Control Vectors

The most elementary switching action selects one of the six MMC arms and switches a single SM capacitor, generating a voltage step of size v_C in that arm. Based on (5)–(8), Table II gives the resulting changes of the cc, dc, ac, and cm voltages.

Fig. 7 presents this information graphically showing the space vector changes for $\underline{v}_{\rm cc}$ and $\underline{v}_{\rm ac}$. In the first row of Fig. 7, each green circle denotes a positive voltage step $+v_C$ in the indicated arm (diagrams No. 1–6). In the second row of Fig. 7, each brown circle signifies a negative voltage step $-v_C$ (diagrams No. 7–12). These 12 interventions (switching a single SM capacitor within the whole MMC) will be called single switching operation (SSO) in the following. In view of the guidelines noted previously, SSOs are first choice for generating control vectors. As can be seen in Fig. 7, each SSO simultaneously affects all control voltages $\underline{v}_{\rm cc}$, $\underline{v}_{\rm ac}$, $v_{\rm dc}$, and $v_{\rm cm}$.

Now, a feasible approach could be to estimate the effects of alternative SSOs on all six variables and to make then an optimal choice, see [33]. This would, however, require some predictive trajectory planning and online computed optimization, which had to be avoided in favor of the short control dead times. Instead, the six variables have been ranked. The highest priority is assigned jointly to the ac and cc variables due to the following reasons.

1) AC ripples have to be reduced as far as possible for achieving a good current quality with small harmonics.
2) CC have to be controlled very tightly in order to enable the reduction of inductances, leading to an enhanced dynamic control bandwidth.

The prioritized cc and ac variables need tight tolerance bands of current and voltage errors, which can be specified. Both variables can simultaneously be adjusted by one SSO, Fig. 7 shows for all 12 SSO options the resulting change of $\underline{v}_{\rm cc}$ (red arrow) and $\underline{v}_{\rm ac}$ (blue arrow). There are six discrete changes of $\underline{v}_{\rm cc}$ and six discrete changes of $\underline{v}_{\rm ac}$. Additionally, there is always a combination where cc and ac are corrected nearly in the same direction (e.g., diagram No. 1), and one where the corrections nearly point into the opposite direction (e.g., diagram No. 4). Thus, there is always at least one specific SSO reducing the magnitude of error both for the ac- and cc-component, having a desired $\underline{v}_{\rm cc}$- and $\underline{v}_{\rm ac}$-effect at the same time. The resulting small crosstalk for the two scalar values can be accepted, as long as they are not driven out of their tolerance band.

The control of $v_{\rm dc}$ is mainly based upon so-called double switching operations (DSOs), where two SM-capacitors of the MMC are simultaneously switched. As shown in Fig. 7, a corresponding DSO (brown circles in diagrams No. 1–6 and

TABLE II
RESULTING VOLTAGE CHANGES OF SSOS

No.	SSO	$\frac{u_{cc,1}}{u_C}$	$\frac{u_{cc,2}}{u_C}$	$\frac{u_{cc,3}}{u_C}$	$\frac{u_{dc}}{u_C}$	$\frac{u_{ac,12}}{u_C}$	$\frac{u_{ac,23}}{u_C}$	$\frac{u_{ac,31}}{u_C}$	$\frac{u_{cm}}{u_C}$
1	$+p_1$	-1	$1/2$	$1/2$	$1/3$	$-1/2$	0	$1/2$	$-1/6$
2	$+p_2$	$1/2$	-1	$1/2$	$1/3$	$1/2$	$-1/2$	0	$-1/6$
3	$+p_3$	$1/2$	$1/2$	-1	$1/3$	0	$1/2$	$-1/2$	$-1/6$
4	$+n_1$	-1	$1/2$	$1/2$	$1/3$	$1/2$	0	$-1/2$	$1/6$
5	$+n_2$	$1/2$	-1	$1/2$	$1/3$	$-1/2$	$1/2$	0	$1/6$
6	$+n_3$	$1/2$	$1/2$	-1	$1/3$	0	$-1/2$	$1/2$	$1/6$
7	$-p_1$	1	$-1/2$	$-1/2$	$-1/3$	$1/2$	0	$-1/2$	$1/6$
8	$-p_2$	$-1/2$	1	$-1/2$	$-1/3$	$-1/2$	$1/2$	0	$1/6$
9	$-p_3$	$-1/2$	$-1/2$	1	$-1/3$	0	$-1/2$	$1/2$	$1/6$
10	$-n_1$	1	$-1/2$	$-1/2$	$-1/3$	$-1/2$	0	$1/2$	$-1/6$
11	$-n_2$	$-1/2$	1	$-1/2$	$-1/3$	$1/2$	$-1/2$	0	$-1/6$
12	$-n_3$	$-1/2$	$-1/2$	1	$-1/3$	0	$1/2$	$-1/2$	$-1/6$

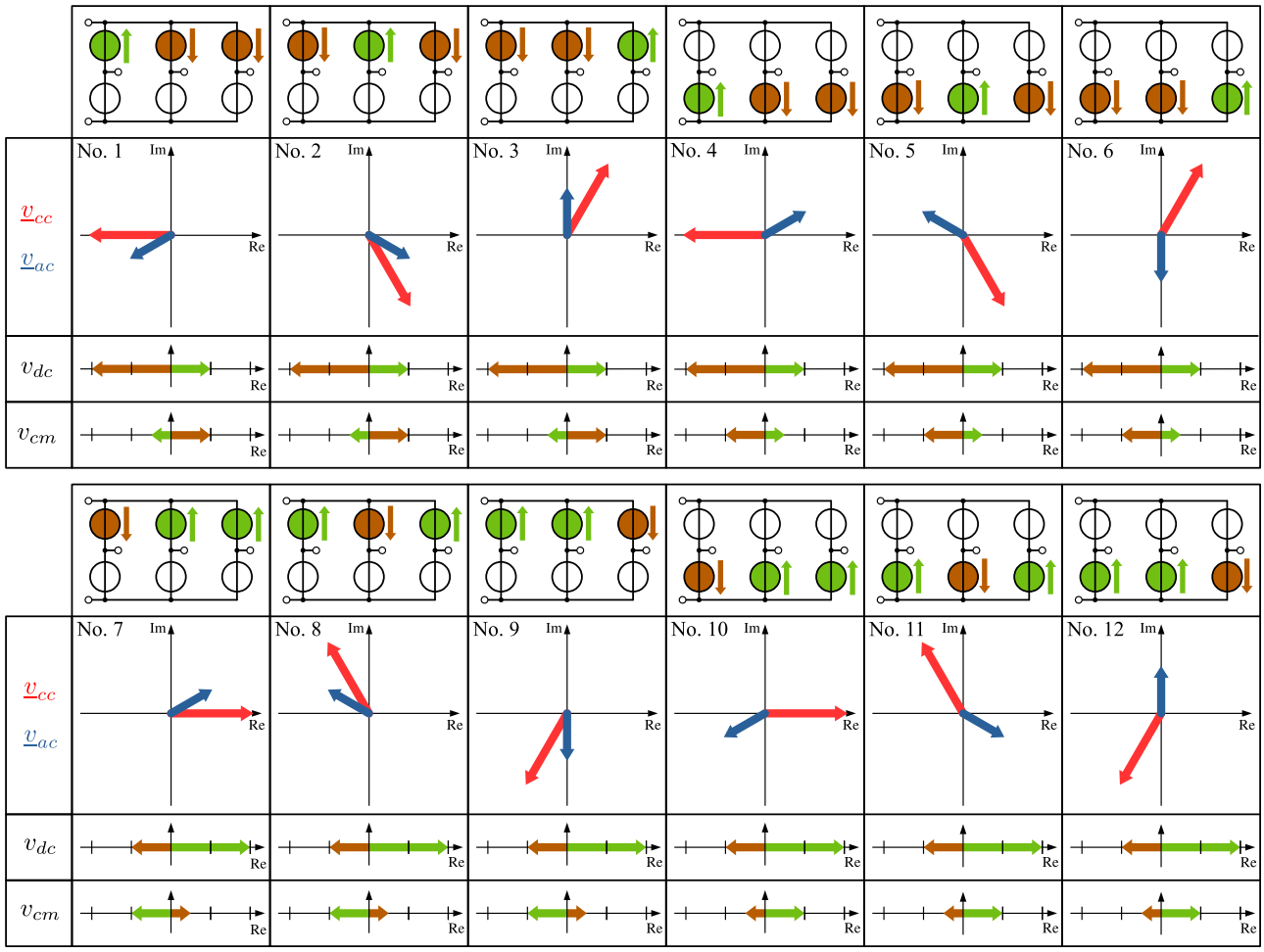

Fig. 7. Single switching operations (SSOs) with the resulting voltage vector changes $\underline{v}_{\mathrm{cc}}$ and $\underline{v}_{\mathrm{ac}}$ and scalar voltage changes v_{dc} and v_{cm}. The extension to double switching operations (DSOs) maintains $\underline{v}_{\mathrm{cc}}$ and $\underline{v}_{\mathrm{ac}}$, but inverts and doubles the amplitude of v_{dc} and v_{cm}.

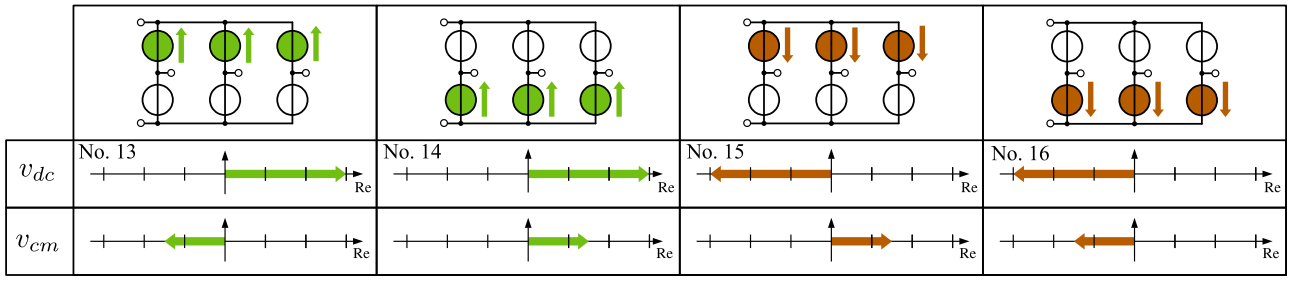

Fig. 8. Triple switching operations (TSOs) with the resulting scalar voltage changes v_{dc} and v_{cm}. These cause only a very small change of the voltage vectors $\underline{v}_{\mathrm{cc}}$ and $\underline{v}_{\mathrm{ac}}$, since the TSO switches SMs with slightly different capacitor voltages.

green circles in diagrams No. 7–12) always exists for each of the 12 SSO options, having the same effect on $\underline{v}_{\mathrm{cc}}$ and $\underline{v}_{\mathrm{ac}}$, but leading to an inverse polarity and a two times higher magnitude of the v_{dc}-correction. So, whenever $\underline{v}_{\mathrm{cc}}$ or $\underline{v}_{\mathrm{ac}}$ need to be adjusted, v_{dc} can additionally be controlled by selecting either the suitable SSO or the corresponding DSO action.

Since v_{cm} does not drive a current, it is assigned the least priority. Compared to cc, ac, and dc, the cm component rarely needs adjustments. Small v_{cm} corrections can be done—in a similar way to dc-voltage control–by replacing an SSO by its corresponding DSO, see Fig. 7 and the passage above. If a larger cm voltage correction should be necessary, a third group of four switching operations can be employed. As shown in Fig. 8, the corresponding voltage changes are generated by simultaneously switching three SMs in the three upper arms or the three lower arms, an action called triple switching operation (TSO). These options allow for simultaneous correction of both scalar values, dc and cm, without affecting $\underline{v}_{\mathrm{cc}}$ and $\underline{v}_{\mathrm{ac}}$.

Based on this set of 28 switching options (12SSO+12DSO+4TSO), reactions to arbitrary error state

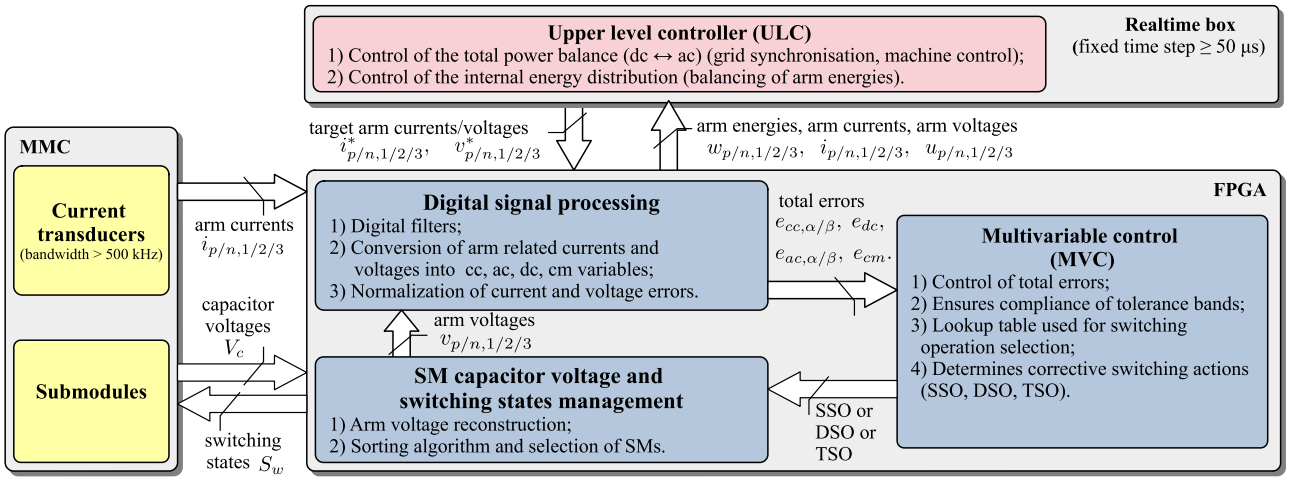

Fig. 9. Simplified signal flow diagram of the hardware setup.

TABLE III
PARAMETERS OF THE HARDWARE SETUP

Name	Value	Unit	Description
n	16		Number of submodules per arm
C	2	mF	Submodule capacitance
$v_{C,nom}$	46	V	Nominal submodule voltage
L_e	1.56	mH	Arm inductance
L_d	1.76	mH	DC-side equivalent inductance
L_a	1.62	mH	AC-side equivalent inductance

TABLE IV
TOLERANCE BAND SETTINGS USED IN ALL EXPERIMENTS

Name	Value	Unit	Description
$i_{cc,tb}$	308	mA	Circulating current tolerance band
$i_{ac,tb}$	386	mA	Alternating current tolerance band
$i_{dc,tb}$	418	mA	Direct current tolerance band
$v_{cc,tb}$	83.3	V	CC voltage tolerance band
$v_{ac,tb}$	48.4	V	AC voltage tolerance band
$v_{dc,tb}$	77.6	V	DC voltage tolerance band
$v_{cm,tb}$	36.2	V	CM voltage tolerance band

combinations of the six variables are analyzed and optimized *offline*, and the optimal switching commands are stored in a lookup table. During the MVC operation, this offline-generated lookup table gets the preprocessed information about the actual error state and directly outputs the best switching decision.

IV. HARDWARE SETUP

With respect to the hardware of MMC, main drivers of progress are advanced SM topologies [38], [39]. These advanced SM topologies enable a significantly improved tradeoff regarding power losses and capacitor size, compared to full-bridge or half-bridge SMs. In consequence the severe drawbacks of half-bridge SMs, especially larger capacitor size, narrow operating range, and lack of overcurrent protection, do not have to be accepted in future. Therefore, the MVC-concept has been designed for these advanced SM topologies, which are equivalent to full-bridge SMs with respect to control functionality. A down scaled MMC prototype with 96 full-bridge SMs has been built (partly developed in [40]) in order to test and validate the presented control concept. General system parameters are listed in Table III.

The simplified signal flow diagram of the hardware setup is shown in Fig. 9. A ULC is employed to control the grids, to maintain the desired power balance of the external connected systems, and to adjust the internal energy distribution, using the concept described in [41]. This controller is implemented in a real-time box, which provides the target arm currents and arm voltages in constant sampling intervalls of 50 μs. Since the current dynamics are much faster than the energy dynamics, the lower-level controller has to assure a much wider bandwidth, as explained. Therefore, the MVC and additional signal processing are implemented on an FPGA. In the first stage, called *digital signal processing*, the target and measured currents/voltages are normalized and transformed into total errors e. These are fed into the MVC. This ensures compliance of specified tolerance bands and outputs one of the predefined switching options from its lookup table. The final selection of those SMs, which have to be switched, is conducted in a separate control stage, which manages SM capacitor balancing. Fiber optical communication is used for bidirectional data transfer between the SMs and FPGA.

Four different experimental results are shown as follows.

1) Section IV-A: Steady-state operation.
2) Section IV-B: Fast changes of target values.
3) Section IV-C: External voltage drop of $v_{\mathrm{dc},ex}$.
4) Section IV-D: Robustness against inaccurate values of external inductances L_d and L_a.

The specified tolerance bands, used in all three scenarios, are given in Table IV.

A. Experimental Results: Steady-State Operation

In a steady-state operation, minimizing the necessary switching frequency, while maintaining high-quality output currents/voltages, is of prime importance. Table V gives the set point used for the steady-state operation. Note that the low frequency

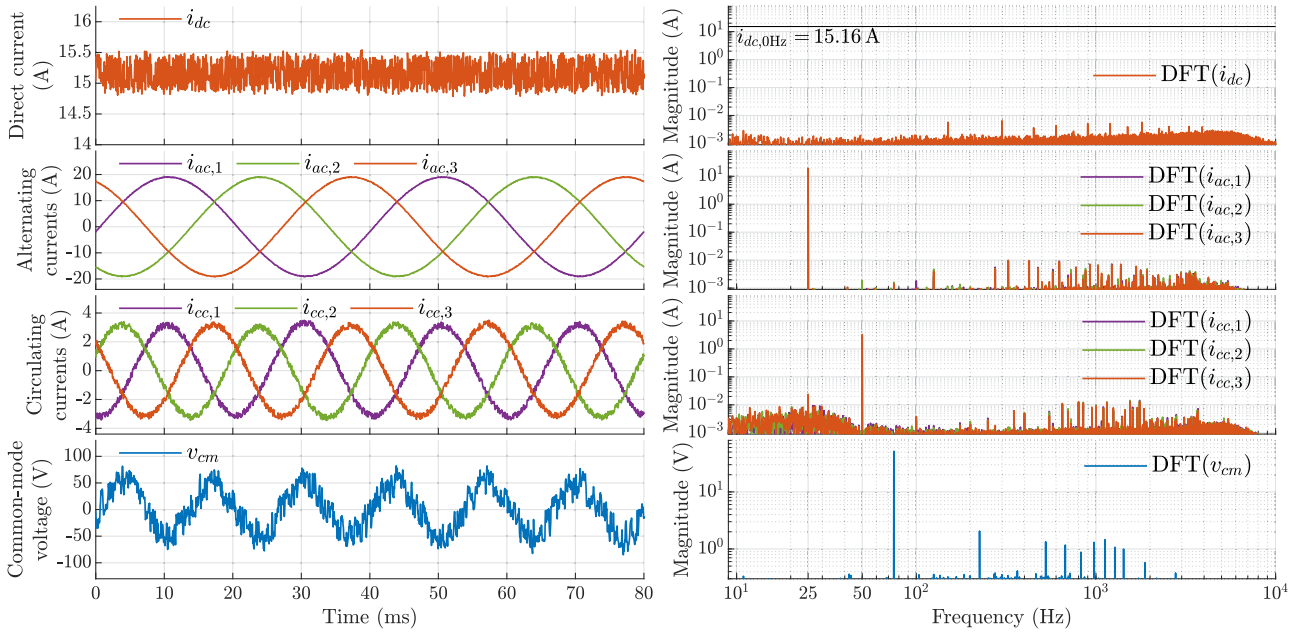

Fig. 10. Experimental results of steady-state discrete Fourier transform (DFT) analysis of all controlled variables. Parameters of the set point are given in Table V. Time duration of analyzed data for the DFT is 12 s.

TABLE V
PARAMETERS AND TARGET VALUES (*) OF THE STEADY-STATE OPERATION

Name	Value	Unit	Description
$v_{dc,ex}$	560	V	External dc voltage
i^*_{dc}	15.13	A	Direct current
p^*_{dc}	8.47	kW	DC-link power
$\hat{i}^*_{ac}$	19	A	Alternating current amplitude
$\hat{v}^*_{ac}$	298	V	Alternating voltage amplitude
$\cos(\varphi)$	1		Power factor
f_1	25	Hz	AC frequency
$\hat{i}^*_{cc}$	3.17	A	Circulating current amplitude
f_{cc}	50	Hz	Circulating current frequency
$\hat{v}^*_{cm}$	49.7	V	Common-mode voltage amplitude
f_{cm}	75	Hz	Common-mode voltage frequency

$f_1 = 25$ Hz and a suboptimal set point

$$k = \frac{\hat{v}_{\text{ac}}}{v_{\text{dc}}/2} \approx 1.06 \qquad (\text{optimal value } \approx 1.25) \tag{11}$$

were chosen to generate larger energy ripples (and therefore SM capacitor voltage ripples) in the arms. (This measure was easier to implement in the present MMC, than a hardware replacement of all 96 SM capacitors.) A typical specification of cc with frequency $2f_1$ is used to reduce the arm energy hub. The cm voltage with frequency $3f_1$ is used to lower the arm voltage peaks. The cc and cm amplitudes are set as follows:

$$\hat{i}^*_{\text{cc}} = \frac{\hat{i}^*_{\text{ac}}}{6}, \qquad \hat{u}^*_{\text{cm}} = \frac{\hat{v}^*_{\text{ac}}}{6}. \tag{12}$$

In Fig. 10, a discrete Fourier transform (DFT) analysis of the six controlled variables is done. In the left column, 80 ms extractions of the signals are shown, while the DFTs are calculated using 12 s of data ($f_s = 20$ kHz). The average switching frequency (relevant for the switching power loss) per semiconductor in the whole MMC is

$$f_{\text{sw}} = \frac{n_{\text{sw}}}{4 \cdot 6nT_{\text{sw}}} = \frac{n_{\text{sw}}}{n_{sc}T_{\text{sw}}}. \tag{13}$$

In (13), n_{sw} denotes the number of switching actions in time interval T_{sw} and n_{sc} is the total number of semiconductors in the MMC. In the experiment, f_{sw} has been 133.6 Hz. Note that the switching frequency is primarily a result of the specified current tolerance bands. A lower/higher switching frequency can easily be achieved by increasing/reducing the current tolerance bands.

All controlled variables are kept within their tolerance bands. The desired fundamental frequency components (spectral lines) at f_1 (ac), $2f_1$ (cc), and $3f_1$ (cm) show significant distances to the noise floor and high spectral purity. Further reducing the tolerance bands will lower the noise floor, if desired.

The SM capacitor voltages during the steady-state operation are shown in Fig. 11. Each plot contains $n = 16$ colored voltage signals and two black-dashed lines, signifying tolerance bands for the capacitor voltages. Whenever a capacitor voltage touches these limits, the corresponding SM is switched into zero state and another SM of the same arm is used as a replacement. The chosen set point results in a voltage ripple of approximately 10 V ($\approx 21\%$ of $v_{C,\text{nom}}$). Due to the permanent correction of voltage and current errors by the MVC, large capacitor voltage ripples are acceptable. Consequently, the installed SM capacitances could be further reduced, if requested.

In Fig. 12, the normalized voltage-, current-, and total errors of scalar components dc and cm are shown. Executed switching operations are indicated through black-dashed lines and appropriate labels of selected arms and the trigger variable. For a deeper understanding of executed switching operations, the time span highlighted in gray is analyzed in detail. During this time span, four control interventions have been performed at times

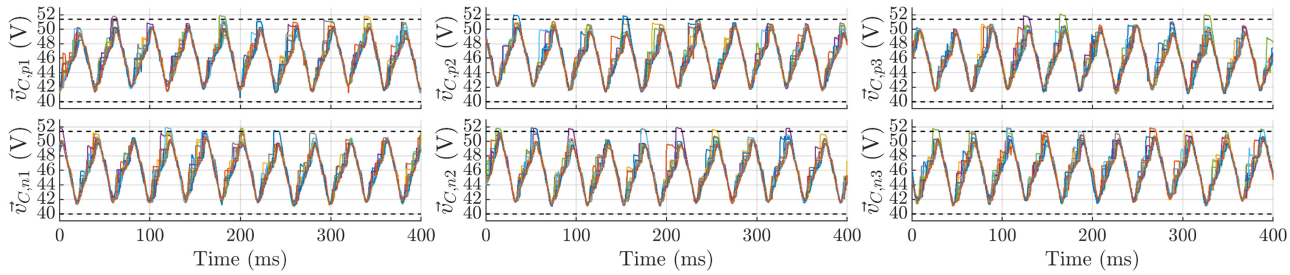

Fig. 11. Experimental results of SM capacitor voltages during steady-state operation. Black-dashed lines denote the tolerance band for the capacitor voltages, which trigger swaps of SMs.

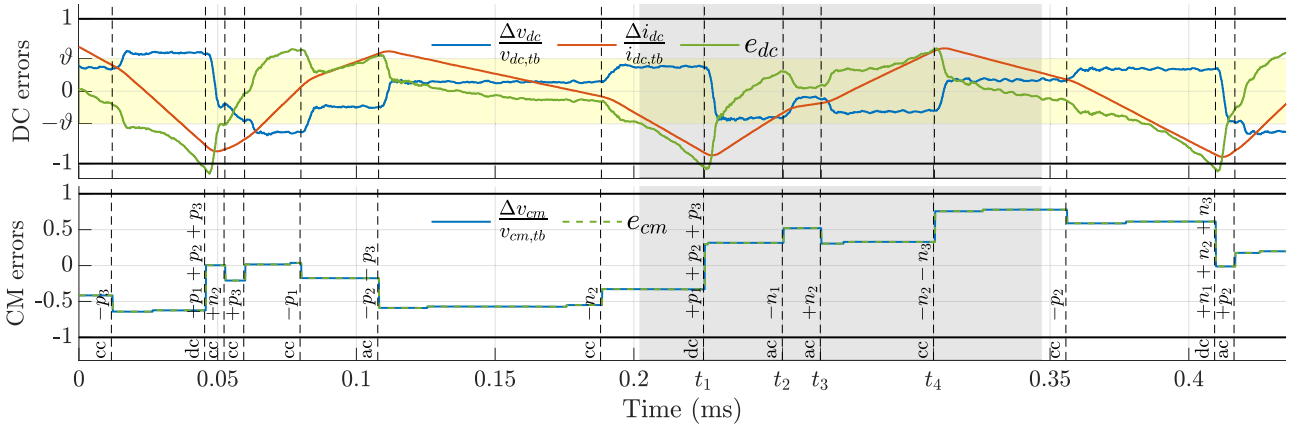

Fig. 12. Experimental results of voltage, current, and total errors of the scalar dc and cm components. Switching actions are denoted by black-dashed lines with labels of switched arms and trigger variable. The gray highlighted time zone includes four switching actions (t_1, t_2, t_3, and t_4), which are analyzed in detail (see Table VI).

TABLE VI
DETAILED SWITCHING OPERATION ANALYSIS OF THE GRAY HIGHLIGHTED TIME SPAN IN FIG. 12

Time	Trigger	Selected operation (see Fig. 7, 8)	Type of execution
$t_1 = 225.1\,\mu s$	dc	No. 13	TSO
$t_2 = 253.5\,\mu s$	ac	No. 10	SSO
$t_3 = 267.2\,\mu s$	ac	No. 5	SSO
$t_4 = 308.0\,\mu s$	cc	No. 4	DSO

t_1, t_2, t_3, and t_4. Detailed information about the exact times, triggers, selected space vectors with respect to Figs. 7 and 8, and the type of execution (SSO, DSO, or TSO) are listed in Table VI. For the highlighted time span of Fig. 12, cc and ac voltage-, current-, and total errors (space vectors) are shown in Fig. 13, including their circle-shaped tolerance bands. Executed switching operations are represented by time-labeled black dots. In the graphs of the voltage errors $\Delta\underline{v}_{cc}$ and $\Delta\underline{v}_{ac}$, additional gray arrows are included, illustrating the theoretical voltage error changes of the selected switching operation with nominal SM capacitor voltage $v_{C,nom}$. Note that the small overshoots in the total errors e are caused by unavoidable, small time delays of the real digital signal processing.

At time t_1, the error e_{dc} exceeds its tolerance band, which leads to a control intervention. An overflow of the dc or cm error is always corrected with a TSO, which simultaneously corrects e_{dc} and e_{cm}. The selection of the appropriate TSO is straightforward and depends on the signs of the errors e_{dc} and e_{cm} only. Since v_{dc} and v_{cm} enter the error terms with a negative sign [see (9) and (10)], they appear inverted in Fig. 12. In this case, $+p_1$, $+p_2$, $+p_3$ (No. 13, see Fig. 8) reduces e_{dc} and e_{cm} in the best manner. Since three slightly different SM capacitor voltages have been switched, a small disturbance of the voltage errors $\Delta\underline{v}_{cc}$ and $\Delta\underline{v}_{ac}$ can be seen in Fig. 13. The absolute value of this disturbing voltage vector is smaller than an SSO, and thus, can be neglected.

At time t_2, the error $\underline{e}_{ac}$ touches its tolerance band, which triggers another control intervention. An error of the cc or ac component is always corrected with a voltage-space vector generated by an SSO (or DSO). All possible options are shown in Fig. 7. Note that these voltage-space vectors represent the change of the actual voltages. (Since these voltages enter the error terms with a negative sign [see (9) and (10)], they appear phase-shifted by 180° in Fig. 13.) Considering the cc and ac errors at time t_2, two possible SSOs could be selected: 1) $+n_2$ (No. 5) or 2) $-n_1$ (No. 10). This opens up the option of controlling an additional variable. In this case, $-n_1$ (No. 10) has been selected, since it lowers the dc error e_{dc}, too. The theoretically determined error voltage changes using this SSO, with angles of 180° for $\Delta\underline{v}_{cc}$ and 30° for $\Delta\underline{v}_{ac}$ (see gray arrows), coincide with the experimental results very well.

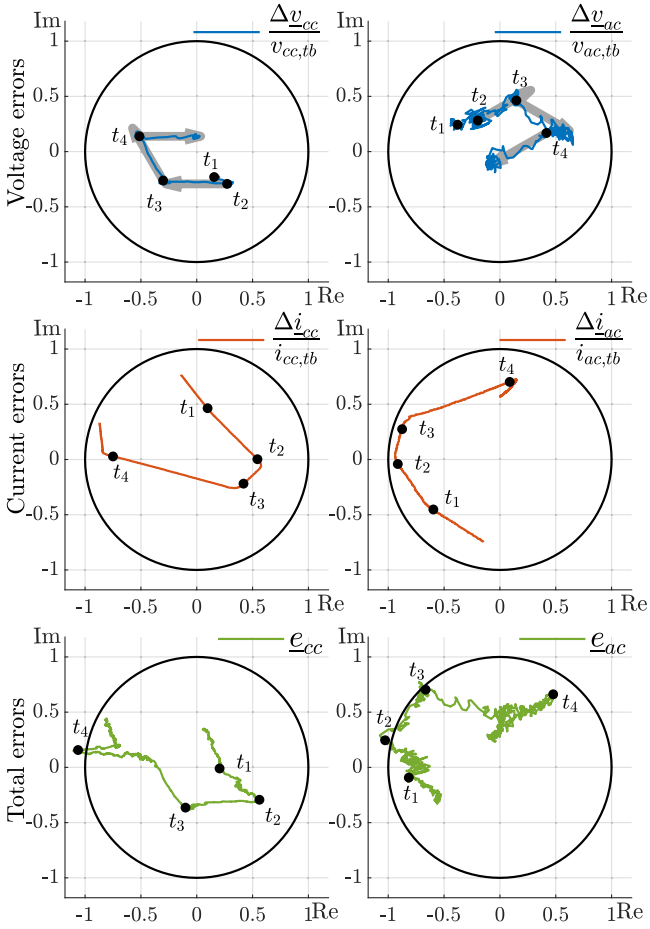

Fig. 13. Experimental results of voltage, current, and total errors of cc and ac components. Labeled black dots (t_1, t_2, t_3, and t_4) represent switching actions in the gray highlighted time span of Fig. 12.

Fig. 14. Lookup table is used to obtain optimal switching decisions based on discretized total errors.

At time t_3, the error $\underline{e}_{\mathrm{ac}}$ touches its tolerance band again and the SSO $+n_2$ (No. 5) is selected.

At time t_4, the error $\underline{e}_{cc}$ touches its tolerance band, which triggers another control intervention. In the first step, the best SSO considering $\Delta\underline{e}_{\mathrm{cc}}$ or $\Delta\underline{e}_{\mathrm{ac}}$ is identified: $+n_1$ (No. 4). Because of the dc-error e_{dc} being larger than ϑ, an extension towards the DSO $-n_2$ and $-n_3$ (No. 4) is selected. The theoretically determined error voltage changes with angles of 0° for $\Delta\underline{v}_{\mathrm{cc}}$ and 210° for $\Delta\underline{v}_{\mathrm{ac}}$ match with the experimental results very well. Using a DSO, in this case, inverts the sign of the dc-error voltage Δv_{dc}, which is advantageous for reducing the number of TSOs and maximizing the time between switching actions (i.e., reducing the switching frequency).

As explained, the switching decisions solely depend on the actual total errors $\underline{e}_{\mathrm{cc}}$, $\underline{e}_{\mathrm{ac}}$, e_{dc}, and e_{cm}. Therefore, a lookup table can be used for the implementation. The integration in the MVC structure is shown in Figs. 5 and 14 . Two significant advantages resulting from using a lookup table are as follows.

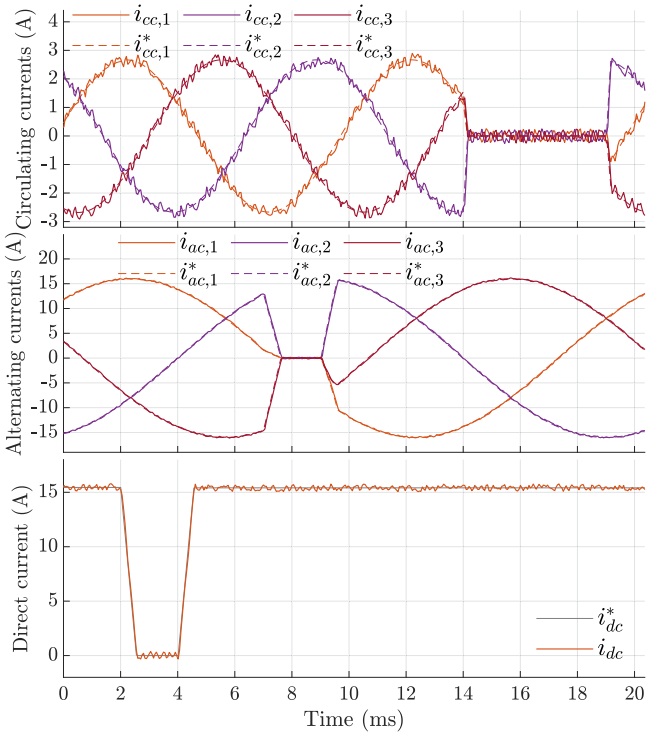

Fig. 15. Experimental results of dynamic target value changes of the dc i_{dc} (15.4 ↔ 0 A), the ac amplitude $\hat{i}_{\mathrm{ac}}$ (16 ↔ 0 A), and the cc amplitude $\hat{i}_{\mathrm{cc}}$ (2.7 ↔ 0 A).

1) The time delay of the selection process is almost zero (below 50 ns).
2) For each error state (input combination), the response has been optimized offline.

Item 2) enables the use of simulation models or experimental data to improve the selection process. Basically, each error state can be analyzed in detail to acquire the explicit best switching decision (SSO, DSO, or TSO). Since the whole MVC concept operates with normalized variables, the lookup table has to be created and optimized once only. There is no dependency on system parameters, such as the number of SMs, the power rating, or other design parameters.

In summary, the derived MVC concept is able to keep all the controlled variables in their tolerance bands under any combination of operating conditions. The switching frequency is minimized, because control interventions solely get triggered when necessary (i.e., when a tolerance band is touched).

B. Experimental Results: Dynamic Performance

MVC is designed to be a solid basis for the ULC, realizing all demanded target values with high accuracy and bandwidth. Especially in case of dynamic target value changes, which are necessary for performing quick energy shifts between the converter arms or sudden adjustments of external power balance, the MVC has to meet these requirements. During these temporary scenarios, minimized dead time is of prime importance.

Fig. 15 shows the measured values while performing a hard drop and recovery of the following quantities.

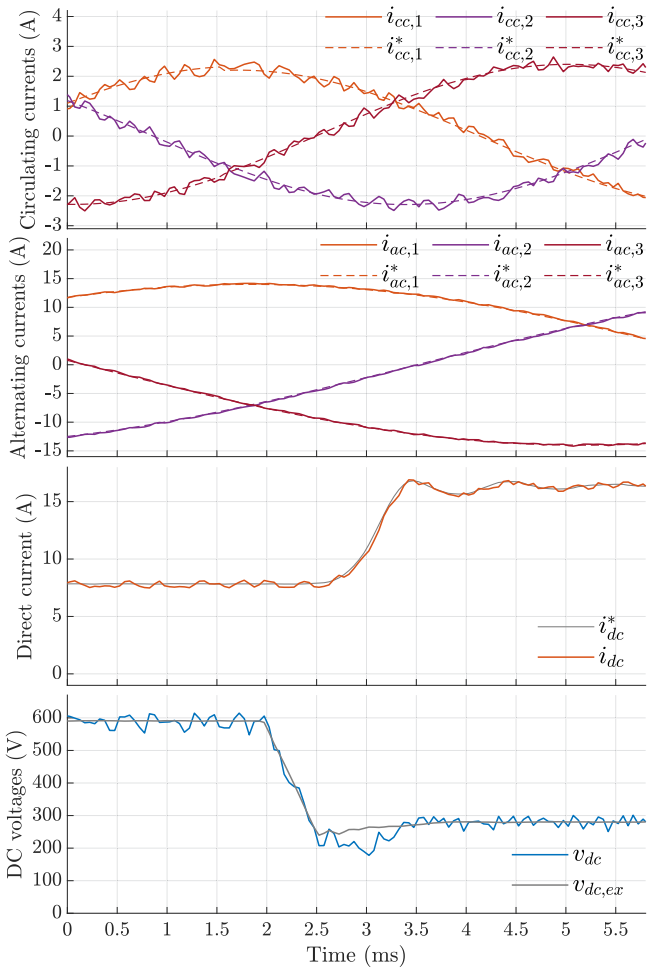

Fig. 16. Experimental results of a sudden external dc voltage $v_{\mathrm{dc,ex}}$ drop (590–280V).

1) DC (15.4 $\leftrightarrow$ 0 A).
2) AC amplitude (16 $\leftrightarrow$ 0 A).
3) CC amplitude (2.7 $\leftrightarrow$ 0 A).

Note that during the drops of i_{dc} and i_{ac}, the powers at the converter terminals are not balanced. The stored energy in the SM capacitors is used to temporarily buffer the real power exchange. Consequently, substantial capacitor voltage changes occur in addition to the dynamic target value changes. MVC proves to be capable of handling these situations. Additionally, independent and simultaneous control of all six controlled variables is assured. Furthermore, the MVC enables the specification of desired current derivatives for each controlled variable within the limits set by arm voltage head room

$$\frac{\mathrm{d}i^*_{\mathrm{dc}}}{\mathrm{d}t} = 28\frac{\mathrm{A}}{\mathrm{ms}}, \quad \frac{\mathrm{d}i^*_{\mathrm{ac}}}{\mathrm{d}t} = 26\frac{\mathrm{A}}{\mathrm{ms}}, \quad \frac{\mathrm{d}i^*_{\mathrm{cc}}}{\mathrm{d}t} = 18\frac{\mathrm{A}}{\mathrm{ms}}. \tag{14}$$

C. Experimental Results: External DC Voltage Drop

Future applications require fully electronic fault management. Especially in the case of external faults in the dc or ac system, MVC has to counteract the occurrence with minimized dead time. Fig. 16 shows experimental results of a sudden external dc voltage $v_{\mathrm{dc,ex}}$ drop from 590 to 280 V. During the time span

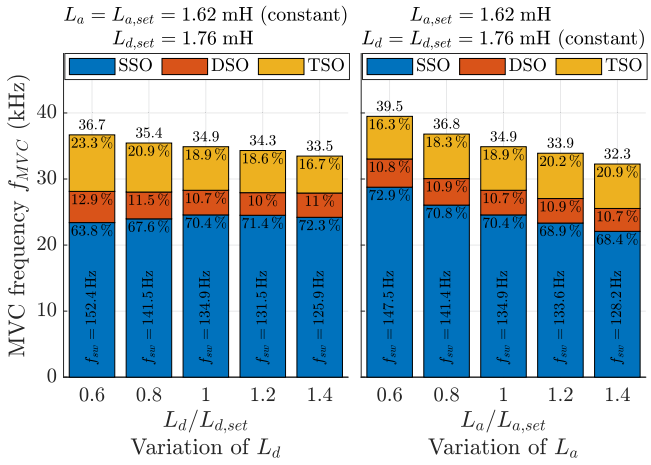

Fig. 17. Control performance with inaccurate values of the equivalent external inductances. L_d and L_a denote the real inductances of the hardware setup. In contrast, the Index set indicates the value the MVC is operating with.

$2\ \mathrm{ms} \leq t \leq 2.5\ \mathrm{ms}$, MVC ensures the strict adherence to given target values. The MVC maintains the target dc i^*_{dc} until an updated target value is provided by the ULC. Therefore, v_{dc} follows the drop in $v_{\mathrm{dc,ex}}$ (see Fig. 3). Note that i^*_{dc} is an output of the upper level controller (ULC), which is responsible for external power balance. Since the ULC operates with a lower controller bandwidth (fixed time step of 50 μs and additional delay of input filters), the target values and, particularly, i^*_{dc} belong to the previous steady state until $t = 2.5$ ms and have not yet been adjusted. In this first stage of the fault, the dc-link power p_{dc} is lower than the ac power p_{ac}, which forces the MMC to utilize its capacitor energy in order to maintain undisturbed ac operation. At time $t = 2.5$ ms, the upper level energy controller begins to adjust the dc target value i^*_{dc} to restore power balance. During this whole incident on the dc-side of the converter, cc and ac variables are not influenced and are precisely following their target values.

D. Experimental Results: Robustness Against Inaccurate Values of External Inductances

Future applications, such as meshed dc-grids, entail a growing complexity of grid models, where parameters may suddenly change. Because of this, one development objective of MVC was to achieve robustness against varying external parameters. The simplified grid model in Fig. 2 contains an equivalent counter voltage and an equivalent inductance, as explained. Robustness against sudden changes of the equivalent counter voltage has been demonstrated in Section IV-C (external dc voltage drop). The robustness against inaccurate values of the equivalent inductances shall be demonstrated now.

Therefore, wrong or mistuned inductance values of L_d and L_a are set within the MVC and the resulting performance is analyzed. Fig. 17 shows the experimental results of $\pm 40\%$ variations of L_d (left-hand side graph) and L_a (right-hand side graph). Additionally, the MVC-frequency f_{MVC}, the semiconductor switching frequency f_{sw}, and the percentage shares of SSO, DSO, and TSO are shown. The switching frequency (being

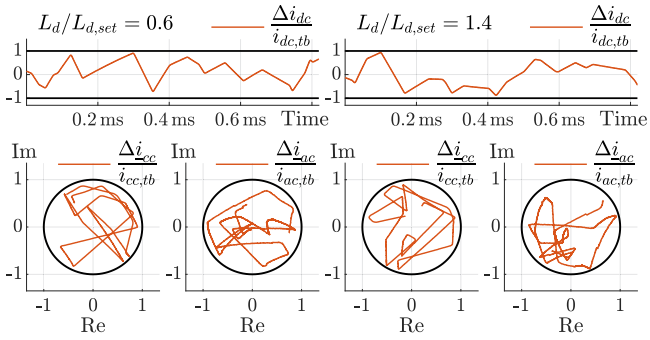

Fig. 18. Current errors (dc, cc, and ac) with -40% (left) and $+40\%$ (right) mistuned inductances at the dc-side.

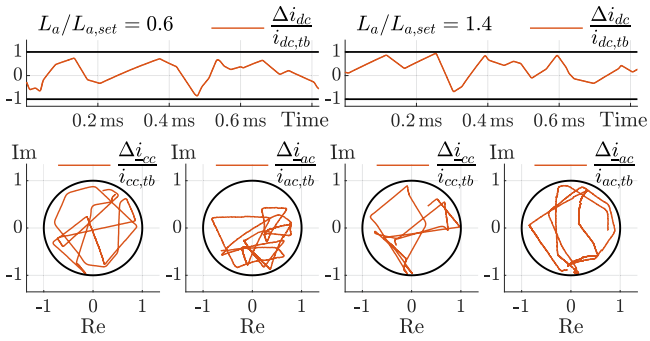

Fig. 19. Current errors (dc, cc, and ac) with -40% (left) and $+40\%$ (right) mistuned inductances at the ac-side.

a measure for semiconductor switching losses) is calculated as

$$f_{\text{sw}} = (1p_{\text{SSO}} + 2p_{\text{DSO}} + 3p_{\text{TSO}})\,\frac{f_{\text{MVC}}}{n_{\text{sc}}} \tag{15}$$

where

p_{SSO} share of SSOs in f_{MVC};
p_{DSO} share of DSOs in f_{MVC};
p_{TSO} share of TSOs in f_{MVC};
f_{MVC} $= \frac{1}{\overline{T}_v}$, with $\overline{T}_v$ being the average time duration between switching interventions of the MVC;
n_{sc} number of semiconductor switches in the MMC.

Decreasing the real inductances L_d and L_a enforces the MVC to moderately increase f_{MVC} and f_{sw}. The physical explanation is that a more accurate and tight control of voltage–time-areas is required to meet the current tolerance band. Looking into the details, it becomes evident that decreasing L_d leads to an increase in TSOs, while the number of SSO plus DSO remain nearly the same. Decreasing L_a leads to an increase of SSOs, while the absolute number of DSOs and TSOs approximately remain the same. As shown in Figs. 18 and 19, even when operating with strongly inaccurate values of the equivalent inductances L_d and L_a, the MVC manages to precisely keep all currents within their tolerance bands.

V. Conclusion

For demanding future applications of MMC, i.e., multiterminal dc grids, a novel control concept (MVC) was presented, explained, and tested, using a down-scaled MMC with 96 SMs. The experimental results demonstrated that the dynamic performance of the control system was improved by more than one order of magnitude—compared to state-of-the-art MMC control. Additionally, it has been proven that this MVC concept enables to meet individually specified, tight tolerance bands for all essential values of the MMC even under unexpected fault conditions. The new concept enables to operate MMCs with large numbers of SMs and to essentially reduce SM capacitors and arm inductances.

Appendix

Transducers and Processing of Measured Values

When increasing the bandwidth of control more than one order of magnitude—compared to the state of the art—the bandwidth and the real performance of the required transducers has to be considered. Because some of the measurement values can be replaced by online models, the focus must be directed on those values, where high bandwidth is mandatory.

At first glance, a concept relying on fast voltage measurements seems to be favorable and easy to implement. Yet, voltage measurements with respect to bandwidth are suffering from basic limitations in these applications. (This represents another difficulty for group A or B control methods, relying on fast voltage measurements.) On the other hand, current measurements do not suffer from these basic limitations. In addition, current measurement is local and its imperfections do not increase when increasing the physical size of the converter and the voltages of the related system. Precision and bandwidth of current measurements are mainly an issue of advanced transducer technology. For the present applications, current sensors based on the *flux gate concept* have reached outstanding performance in the last years [42], [43].

In conclusion, it was decided to base the MVC concept solely on arm current measurements and to avoid direct measurements of the voltage errors, by replacing them by estimated di/dt errors, as described. A satisfying quality of these error signals could be achieved, by applying a digital FIR-filter operating with a sampling frequency of $f_s = 10$ MHz, realized in the FPGA. The order of this digital filter can be freely chosen. In the present setup, the order $n_o = 50$ has been chosen as a reasonable compromise between quality and signal delay. The experimental results clearly demonstrate that the quality of the generated error signals is fully sufficient for stable operation of the MMC (i.e., Fig. 13).

References

[1] R. Marquardt, "Modular multilevel converters: State of the art and future progress," *IEEE Power Electron. Mag.*, vol. 5, no. 4, pp. 24–31, Dec. 2018.
[2] M. A. Perez, S. Bernet, J. Rodriguez, S. Kouro, and R. Lizana, "Circuit topologies, modeling, control schemes, and applications of modular multilevel converters," *IEEE Trans. Power Electron.*, vol. 30, no. 1, pp. 4–17, Jan. 2015.
[3] S. Rivera, B. Wu, R. Lizana, S. Kouro, M. Perez, and J. Rodriguez, "Modular multilevel converter for large-scale multistring photovoltaic energy conversion system," in *Proc. IEEE Energy Convers. Congr. Expo.*, 2013, pp. 1941–1946.

[4] K. Sharifabadi, L. Harnefors, H.-P. Nee, S. Norrga, and R. Teodorescu, *Design, Control, and Application of Modular Multilevel Converters for HVdc Transmission Systems*. Piscataway, NJ, USA: IEEE Press, 2016.
[5] M. Spichartz, V. Staudt, and A. Steimel, "Modular multilevel converter for propulsion system of electric ships," in *Proc. IEEE Electric Ship Technol. Symp.*, 2013, pp. 237–242.
[6] J. A. Ansari, C. Liu, and S. A. Khan, "MMC based MTDC grids: A detailed review on issues and challenges for operation, control and protection schemes," *IEEE Access*, vol. 8, pp. 168154–168165, Sep. 2020.
[7] J. Freytes *et al.*, "Dynamic analysis of MMC-based MTDC grids: Use of MMC energy to improve voltage behavior," *IEEE Trans. Power Del.*, vol. 34, no. 1, pp. 137–148, Feb. 2019.
[8] S. Debnath, J. Qin, B. Bahrani, M. Saeedifard, and P. Barbosa, "Operation, control, and applications of the modular multilevel converter: A review," *IEEE Trans. Power Electron.*, vol. 30, no. 1, pp. 37–53, Jan. 2015.
[9] A. Dekka, B. Wu, R. L. Fuentes, M. Perez, and N. R. Zargari, "Evolution of topologies, modeling, control schemes, and applications of modular multilevel converters," *IEEE Trans. Emerg. Sel. Topics Power Electron.*, vol. 5, no. 4, pp. 1631–1656, Dec. 2017.
[10] P. Münch, D. Görges, M. Izák, and S. Liu, "Integrated current control, energy control and energy balancing of modular multilevel converters," in *Proc. 36th Annu. Conf. IEEE Ind. Electron. Soc.*, 2010, pp. 150–155.
[11] P. Münch, S. Liu, and G. Ebner, "Multivariable current control of modular multilevel converters with disturbance rejection and harmonics compensation," in *Proc. IEEE Int. Conf. Control Appl.*, 2010, pp. 196–201.
[12] T. Geyer, *Model Predictive Control of High Power Converters and Industrial Drives*. Hoboken, NJ, USA: Wiley, 2017.
[13] A. Gensior and H. Fehr, "Modeling and energy balancing control of modular multilevel converters using perturbation theory for quasi-periodic systems," *IEEE Trans. Power Electron.*, vol. 36, no. 2, pp. 2201–2217, Feb. 2021.
[14] H. Bärnklau, A. Gensior, and J. Rudolph, "A model-based control scheme for modular multilevel converters," *IEEE Trans. Ind. Electron.*, vol. 60, no. 12, pp. 5359–5375, Dec. 2013.
[15] P. M. Meshram and V. B. Borghate, "A simplified nearest level control (NLC) voltage balancing method for modular multilevel converter (MMC)," *IEEE Trans. Power Electron.*, vol. 30, no. 1, pp. 450–462, Jan. 2015.
[16] P. Hu and D. Jiang, "A level-increased nearest level modulation method for modular multilevel converters," *IEEE Trans. Power Electron.*, vol. 30, no. 4, pp. 1836–1842, Apr. 2015.
[17] A. Hassanpoor, L. Ängquist, S. Norrga, K. Ilves, and H.-P. Nee, "Tolerance band modulation methods for modular multilevel converters," *IEEE Trans. Power Electron.*, vol. 30, no. 1, pp. 311–326, Jan. 2015.
[18] S. Rohner, S. Bernet, M. Hiller, and R. Sommer, "Modulation, losses, and semiconductor requirements of modular multilevel converters," *IEEE Trans. Ind. Electron.*, vol. 57, no. 8, pp. 2633–2642, Aug. 2010.
[19] M. Hagiwara and H. Akagi, "Control and experiment of pulsewidth-modulated modular multilevel converters," *IEEE Trans. Power Electron.*, vol. 24, no. 7, pp. 1737–1746, Jan. 2009.
[20] Y. Deng and R. G. Harley, "Space-vector versus nearest-level pulse width modulation for multilevel converters," *IEEE Trans. Power Electron.*, vol. 30, no. 6, pp. 2962–2974, Jun. 2015.
[21] Y. Deng, Y. Wang, K. H. Teo, M. Saeedifard, and R. G. Harley, "Optimized control of the modular multilevel converter based on space vector modulation," *IEEE Trans. Power Electron.*, vol. 33, no. 7, pp. 5697–5711, Jul. 2018.
[22] A. Dekka, B. Wu, N. R. Zargari, and R. L. Fuentes, "A space-vector PWM-based voltage-balancing approach with reduced current sensors for modular multilevel converter," *IEEE Trans. Ind. Electron.*, vol. 63, no. 5, pp. 2734–2745, May 2016.
[23] A. Hassanpoor, S. Norrga, H. Nee, and L. Ängquist, "Evaluation of different carrier-based PWM methods for modular multilevel converters for HVDC application," in *Proc. 38th Annu. Conf. IEEE Ind. Electron. Soc.*, 2012, pp. 388–393.
[24] B. Li, R. Yang, D. Xu, G. Wang, W. Wang, and D. Xu, "Analysis of the phase-shifted carrier modulation for modular multilevel converters," *IEEE Trans. Power Electron.*, vol. 30, no. 1, pp. 297–310, Jan. 2015.
[25] K. Ilves, L. Harnefors, S. Norrga, and H. Nee, "Analysis and operation of modular multilevel converters with phase-shifted carrier PWM," *IEEE Trans. Power Electron.*, vol. 30, no. 1, pp. 268–283, Jan. 2015.
[26] R. Darus, G. Konstantinou, J. Pou, S. Ceballos, and V. G. Agelidis, "Comparison of phase-shifted and level-shifted PWM in the modular multilevel converter," in *Proc. Int. Power Electron. Conf.*, 2014, pp. 3764–3770.
[27] A. Dekka, B. Wu, V. Yaramasu, R. L. Fuentes, and N. R. Zargari, "Model predictive control of high-power modular multilevel converters-an overview," *IEEE Trans. Emerg. Sel. Topics Power Electron.*, vol. 7, no. 1, pp. 168–183, Mar. 2019.
[28] Z. Gong, P. Dai, X. Yuan, X. Wu, and G. Guo, "Design and experimental evaluation of fast model predictive control for modular multilevel converters," *IEEE Trans. Ind. Electron.*, vol. 63, no. 6, pp. 3845–3856, Jun. 2016.
[29] J. Böcker, B. Freudenberg, A. The, and S. Dieckerhoff, "Experimental comparison of model predictive control and cascaded control of the modular multilevel converter," *IEEE Trans. Power Electron.*, vol. 30, no. 1, pp. 422–430, Jan. 2015.
[30] B. S. Riar, T. Geyer, and U. K. Madawala, "Model predictive direct current control of modular multilevel converters: Modeling, analysis, and experimental evaluation," *IEEE Trans. Power Electron.*, vol. 30, no. 1, pp. 431–439, Jan. 2015.
[31] D. Zhou, S. Yang, and Y. Tang, "Model-predictive current control of modular multilevel converters with phase-shifted pulsewidth modulation," *IEEE Trans. Ind. Electron.*, vol. 66, no. 6, pp. 4368–4378, Jun. 2019.
[32] X. Gao, W. Tian, Y. Pang, and R. Kennel, "Model predictive control for modular multilevel converters operating at wide frequency range with a novel cost function," *IEEE Trans. Ind. Electron.*, vol. 69, no. 6, pp. 5569–5580, Jun. 2022.
[33] D. Dinkel, C. Hillermeier, and R. Marquardt, "Direct multivariable control of modular multilevel converters," in *Proc. 20th Eur. Conf. Power Electron. Appl.*, 2018, pp. P.1–P.10.
[34] D. Dinkel, C. Hillermeier, and R. Marquardt, "Direct multivariable control of MMC under transient conditions," in *Proc. 21st Eur. Conf. Power Electron. Appl.*, 2019, pp. P.1–P.10.
[35] D. Dinkel, C. Hillermeier, and R. Marquardt, "Direct multivariable control for MMC: Digital signal processing and experimental results," in *Proc. 22nd Eur. Conf. Power Electron. Appl.*, 2020, pp. 1–9.
[36] D. Schröder, *Leistungselektronische Schaltungen*. Berlin, Germany: Springer, 2012.
[37] T. Dhaene and D. de Zutter, "Selection of lumped element models for coupled lossy transmission lines," *IEEE Trans. Comput.-Aided Des. Integr. Circuits Syst.*, vol. 11, no. 7, pp. 805–815, Jul. 1992.
[38] K. Ilves, L. Bessegato, L. Harnefors, S. Norrga, and H. Nee, "Semi-full-bridge submodule for modular multilevel converters," in *Proc. 9th Int. Conf. Power Electron. ECCE Asia*, 2015, pp. 1067–1074.
[39] C. Dahmen, F. Kapaun, and R. Marquardt, "Analytical investigation of efficiency and operating range of different modular multilevel converters," in *Proc. IEEE 12th Int. Conf. Power Electron. Drive Syst.*, 2017, pp. 336–342.
[40] M. Galek, "M2C-converter auf basis von MOS-transistoren für Niederspannungsnetzwerke," Ph.D. dissertation, Dept. Elect. Eng. Inf. Technol., Univ. Bundeswehr Munich, Neubiberg, Germany, 2016.
[41] J. Kolb, F. Kammerer, and M. Braun, "Straight forward vector control of the modular multilevel converter for feeding three-phase machines over their complete frequency range," in *Proc. 37th Annu. Conf. IEEE Ind. Electron. Soc.*, 2011, pp. 1596–1601.
[42] *Product Manual: Ultra-Stable High Precision Current Transducers*, version 1.2, Danisense, Taastrup, Denmark.
[43] LEM International SA, "High Precision Current Transducers Catalogue, Publication CAE110901/0," LEM Int. SA, Geneva, Switzerland.

Daniel Dinkel (Member, IEEE) received the B.Sc. and M.Sc. degrees in electrical engineering and information technology from the University of the Bundeswehr Munich, Neubiberg, Germany, in 2013 and 2015, respectively.

He is currently a Scientific Assistant with the Chair of Automation and Control Engineering, University of the Bundeswehr Munich. His research interests include modular multilevel converters (MMCs) and dc/ac grids, with a focus on advanced control strategies and development of hardware prototypes.

Claus Hillermeier received the M.Sc. and Ph.D. degrees in physics from the Ludwig Maximilians Universität, Munich, Germany, in 1987 and 1992, respectively, and the Habilitation degree in mathematics with a treatise on nonlinear multiobjective optimization from the Technical University of Munich, Munich, Germany, in 1999.

From 1992 to 1994, he worked in a project investigating speech recognition with neural networks, before joining, in 1995, the Central Research Department of Siemens Company, where he was a project Scientist, and later on, a project Leader and Principal Research Scientist engaged in modeling, optimization, and control of technical systems. In 2002, he was appointed as a Professor of automation and control engineering with the University of the Bundeswehr, Munich, Germany. From 2003 to 2015, he was one of the founding editors of the book series *Mathematical Engineering* by Springer International Publishing AG. His research interests include methods for nonlinear control, optimization and model-based diagnosis as well as modeling, and control of power electronic systems.

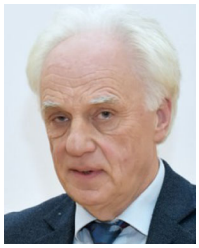

Rainer Marquardt (Member, IEEE) received the M.Sc. and Ph.D. degrees in electronic communication and power electronics from the University of Hannover, Hanover, Germany, in 1978 and 1982, respectively.

Until October 1983, he was a Research Scientist with the Institute for Power Electronics, University of Hannover, under the supervision of Prof. Klemens Heumann. He then joined Siemens AG, Erlangen, as an R&D Engineer and also a Leader of power electronics development of traction and innovation for power electronics. He is currently an "Excellent Emeritus" with the University of the Bundeswehr Munich, Bavaria, Germany, and the Director of the associated Research Institute ITIS. He performed numerous industrial research and development projects for high-power applications in power transmission and advanced ac-drive systems for traction applications. He has filed more than 50 patents in these areas. His inventions include low-loss snubber circuits for gate turn off power semiconductors—first applied in high-speed trains (ICE, Germany) and modular multilevel converters for high-performance/high-power VSC—first applied in HVDC-transmission (San Francisco Bay).

Dr. Marquardt was the recipient of the Highest Award "Ring of Honor" from the Institution of German Electrical Engineers (VDE 2012), the Outstanding Achievement Award from the European Power Electronics Association (EPE 2015), the Uno Lamm HVDC Award from the IEEE (PES 2015), and the William E. Newell Award from the IEEE (PES 2018).